

# SIMULATIONS OF ULTRA-HIGH-ENERGY COSMIC RAYS PROPAGATION

*O. E. Kalashev*<sup>a\*</sup>, *E. Kido*<sup>b\*\*</sup>

<sup>a</sup>*Institute for Nuclear Research, Russian Academy of Sciences  
117312, Moscow, Russia*

<sup>b</sup>*Institute for Cosmic Ray Research, University of Tokyo  
Kashiwa, Chiba, Japan*

Received November 8, 2014

We compare two techniques for simulation of the propagation of ultra-high-energy cosmic rays (UHECR) in intergalactic space: the Monte Carlo approach and a method based on solving transport equations in one dimension. For the former, we adopt the publicly available tool CRPropa and for the latter we use the code TransportCR, which has been developed by the first author and used in a number of applications, and is made available online with publishing this paper. While the CRPropa code is more universal, the transport equation solver has the advantage of a roughly 100 times higher calculation speed. We conclude that the methods give practically identical results for proton or neutron primaries if some accuracy improvements are introduced to the CRPropa code.

DOI: 10.7868/S0044451015050055

## 1. INTRODUCTION

Identification of the origin of ultra-high-energy cosmic rays is one of the main problems of modern astrophysics. Although the existence of particles with the energy  $E \gtrsim 10^{19}$  eV has been confirmed by several experiments, their possible sources, propagation mechanism, and even their nature are still subjects of intense research. Noticeable progress has been achieved during the last decade by the new-generation experiments. A suppression of the cosmic-ray flux above  $E \approx 4 \cdot 10^{19}$  eV has been observed by HiRes, Telescope Array [1], and Pierre Auger Observatories [2, 3]. Depending on the assumed ultra-high-energy cosmic rays (UHECR) composition, this may indicate either the observation of the GZK effect [4, 5] or a natural cut-off in the energy of cosmic-ray sources. The measurements of the position of the shower maximum and its fluctuations by the Pierre Auger experiment suggest a significant fraction of heavy nuclei above  $10^{19}$  eV [6]. However, both composition and energy spectrum studies by HiRes [7] and Telescope Array [8] show consistency with the pure

proton or light-element composition in the same energy range.

Ultra-high-energy protons and nuclei cannot be kept by the galactic magnetic field and therefore freely escape the galaxy. Currently, there are no known sources within the Milky Way that could possibly accelerate protons or nuclei to ultra-high energies, and it is therefore assumed that the particles should have extragalactic origin. During their propagation through intergalactic space, UHECRs rapidly lose energy in interactions with the intergalactic photon background. Understanding the UHECR attenuation process is crucial for making model predictions and interpreting experimental results.

Many studies on propagation of ultra-high-energy nucleons and nuclei exist in the literature, including analytic solutions of the transport equations, which can be found for some specific situations, such as the propagation of nucleons near the GZK cutoff (see, e. g., [9–12]) or using the continuous energy loss (CEL) approximation (see, e. g., [13–15]). Due to the small inelasticity, the CEL approximation works well for  $e^+e^-$  pair production by protons and nuclei. But for pion production on a photon background, due to its large inelasticity and stochastic nature, the CEL approximation predicts a sharper pile-up right below the

\*E-mail: kalashev@inr.ac.ru

\*\*E-mail: ekido@icrr.u-tokyo.ac.jp

GZK cutoff compared to exact solutions [16]. Numerical solutions for nucleons solve the transport equations either directly [16–20] or through Monte Carlo simulation [21–25]. In Ref. [26] (see also references therein), a universal approach to the simulation of cosmic ray propagation is discussed based on the adjoint cascade theory. The photodisintegration of ultra-high-energy nuclei was first discussed in [27] and later in [19, 20, 22, 24, 25, 28, 29].

Unfortunately most of the numerical codes mentioned above are not public. The mutual checks between different propagation codes show a consistency level of about 10%. Due to the growing experimental statistics, improving the simulation accuracy becomes crucial. In this paper, we focus on predictions of the spectra from proton sources. We describe in detail our transport-equation-solving code, which has already been used in a number of works [19], although has not been publicly available until now. We compare our tool with the actively developed Monte Carlo code CRPropa [25], which is publicly available and used in the Pierre Auger Collaboration analysis [30]. While the former code benefits exceedingly high calculation speed, the latter is more universal and easy customizable. In Sec. 2, we discuss the simulation techniques on which the codes are based. In Sec. 3, we compare the results of proton propagation simulations and suggest improvements to CRPropa. Finally, we make a conclusion.

## 2. CALCULATION OF OBSERVABLE SPECTRA

Calculations of the observable UHECR spectra for given production scenarios involve simulation of sources and attenuation effects such as interactions of cosmic rays with intergalactic media and their deflection by galactic and intergalactic magnetic fields. The interaction rate calculation accuracy depends on our knowledge of the infrared intergalactic photon background and its evolution, while particle trajectory calculations rely on the models of intergalactic and galactic magnetic fields. Neither of the above factors is currently known sufficiently well to make definitive predictions. On the other hand, identifying UHECR sources would help constrain the properties of intragalactic media, which especially applies to magnetic field estimates. Our present knowledge of the intergalactic magnetic field (IGMF) is very poor. The theoretical and observational constraints on the mean IGMF strength  $B$

and the correlation length  $L_{cor}$  are summarized in review [31]:

$$10^{-17} \text{ G} \lesssim B \lesssim 10^{-9} \text{ G}, \quad (1)$$

$$L_{cor} \gtrsim 1 \text{ pc}. \quad (2)$$

The simulation assuming the magnetic field growth in a magnetohydrodynamical amplification process driven by structure formation out of a magnetic seed field present at high redshift [32], suggests the present IGMF strength  $B \lesssim 10^{-12} \text{ G}$  (see also Ref. [33]). It can be shown (see, e. g., Ref. [34]) that the effect of magnetic fields on the average energy spectrum of protons with energies  $E \gtrsim 10^{18} \text{ eV}$  is negligible for the IGMF strengths  $B \lesssim 10^{-10} \text{ G}$  (assuming  $L_{cor} \lesssim 1 \text{ Mpc}$ ) if the average distance between the UHECR sources does not exceed the GZK radius. If these conditions are realized, the computation of the averaged fluxes can be done by solving the coupled Boltzmann equations for UHECR transport in one spatial dimension or using one-dimensional Monte Carlo simulation (the first method is usually much faster). In the limit of strong magnetic fields, when it is important to follow particle trajectories, e. g., for calculating the images of discrete sources of UHECR, only the full 3D Monte Carlo simulation can give reliable results. Our code [19] uses the formalism of transport equations, while the CRPropa [25] implements either 1D or 3D Monte Carlo simulations. Below, we describe the CRPropa code only briefly and pay more attention to the transport equation solution.

### 2.1. CRPropa

CRPropa [25] is a Monte Carlo simulation tool aimed at studying the propagation of neutrons, protons, and nuclei in the intergalactic medium. It provides a one-dimensional (1D) and a three-dimensional (3D) modes. In the 3D mode, the magnetic field and source distributions can be defined on a 3D grid. This allows performing simulations in the source scenarios with a highly structured magnetic field configuration. In the 1D mode, magnetic fields can be specified as functions of the distance to the observer, but their effects are restricted to energy losses of electrons and positrons due to synchrotron radiation within electromagnetic cascades. Furthermore, in the 1D mode, it is possible to specify the cosmological source evolution as well as the redshift scaling of the background light intensity. All important interactions with the cosmic infrared (IRB) and microwave (CMB) background light

are included, namely, production of electron–positron pairs, photopion production, and neutron decay. Additionally, CRPropa allows tracking and propagating secondary  $\gamma$ -rays,  $e^+e^-$  pairs, and neutrinos. The code also contains a module solving one-dimensional transport equations for electromagnetic cascades initiated by electrons, positrons, or photons, taking pair production and inverse Compton scattering and synchrotron radiation of electrons into account. For more details on the code, we refer the reader to the Ref. [25].

## 2.2. Transport code

The code developed in [19] simulates attenuation of protons, neutrons, nuclei, photons, and stable leptons by solving the transport equation in one dimension taking all standard dominant processes into account. Ultra-high-energy particles lose their energy in interactions with the electromagnetic background, which consists of CMB, IRB, and radio components (the last effects the electromagnetic cascade development only at ultra-high energies). For IRB backgrounds, several models are implemented [35–40]. For highest-energy protons, neutrons, and nuclei, the main attenuation process is photopion production. Below the photopion production threshold, photodisintegration (for nuclei only) and  $e^+e^-$  pair production provide the attenuation mechanism. Although the attenuation of nuclei is implemented in the code (we use photodisintegration rates derived in [41]), a reliable description of the propagation of heavy nuclei can be achieved only for energies  $E > 10^{19}$  eV (assuming  $B \lesssim 10^{-10}$  G) because deflections in magnetic fields cannot be precisely described within the 1D transport equation formalism. Below, we focus on proton and neutron propagation simulations. With the photopion production by protons and neutrons,  $e^+e^-$  pair production by protons on background photons, and the neutron decay included, the transport equations for protons and nucleons can be written in the form (here and below, we set  $\hbar = c = 1$ ):

$$\begin{aligned} \partial_t N_p(E_p) = & -N_p(E_p) \int d\epsilon n(\epsilon) \times \\ & \times \int d\mu \frac{1 - \beta_p \mu}{2} (\sigma_{p,\pi} + \sigma_{p,e}) + \\ & + \int dE'_p N_p(E'_p) \int d\epsilon n(\epsilon) \int d\mu \frac{1 - \beta'_p \mu}{2} \times \\ & \times \left( \frac{d\sigma_{p,\pi}}{dE_p} + \frac{d\sigma_{p,e}}{dE_p} \right) + \int dE'_n N_n(E'_n) \int d\epsilon n(\epsilon) \int d\mu \times \\ & \times \frac{1 - \beta'_n \mu}{2} \frac{d\sigma_{n,\pi}}{dE_p} + N_n(E_p) \frac{m_n}{E_p} \tau_n^{-1} + Q_p(E_p), \quad (3) \end{aligned}$$

$$\begin{aligned} \partial_t N_n(E_n) = & -N_n(E_n) \int d\epsilon n(\epsilon) \times \\ & \times \int d\mu \frac{1 - \beta_n \mu}{2} \sigma_{n,\pi} + \int dE'_p N_p(E'_p) \times \\ & \times \int d\epsilon n(\epsilon) \int d\mu \frac{1 - \beta'_p \mu}{2} \frac{d\sigma_{p,\pi}}{dE_n} + \\ & + \int dE'_n N_n(E'_n) \int d\epsilon n(\epsilon) \int d\mu \frac{1 - \beta'_n \mu}{2} \times \\ & \times \frac{d\sigma_{n,\pi}}{dE_n} - N_n(E_n) \frac{m_n}{E_n} \tau_n^{-1} + Q_n(E_n), \quad (4) \end{aligned}$$

where  $N_p(E)$  and  $N_n(E)$  are densities of protons and neutrons per unit energy. Here, an isotropic distribution of background photons is assumed with the number density  $n(\epsilon)$  depending on the photon energy  $\epsilon$  only,  $\beta_p$  and  $\beta_n$  are particle velocities,  $\mu$  is the collision angle cosine, and  $Q$  denotes external source terms. The terms describing neutron decay are proportional to  $\tau_n^{-1}$ , the inverse neutron lifetime in the rest frame. In the neutron decay term in Eq. (3), we neglect the difference in masses of the neutron and proton and assume that the recoiling proton momentum is zero in the neutron rest frame. The terms proportional to  $\sigma_{p,\pi}$  and  $\sigma_{n,\pi}$  describe the photopion production by protons and neutrons. Here, we take into account that the nature of the leading nucleon can be changed in the above interaction. Finally, terms proportional to  $\sigma_{p,e}$  describe  $e^+e^-$  pair production by protons.

To solve the above equations numerically, we bin the energies of the cosmic rays. We divide each decade of energy into  $n_d$  equidistant logarithmic bins. We let  $E_i$  denote the central value of the  $i$ th bin, and  $E_{i-1/2}$  and  $E_{i+1/2}$  denote boundary values. Then we rewrite Eqs. (3), (4) in terms of the numbers of particles in each bin

$$N_{p(n),i} = \int_{E_{i-1/2}}^{E_{i+1/2}} N_{p(n)}(E) dE. \quad (5)$$

After replacing the integrals by finite sums, we have

$$\begin{aligned} \frac{d}{dt} N_{p,i} = & -N_{p,i} A_{p,i} + \sum_{j \geq i} B_{p \rightarrow p,ji} N_{p,j} + \\ & + \sum_{j \geq i} B_{n \rightarrow p,ji} N_{n,j} + Q_{p,i}, \quad (6) \end{aligned}$$

$$\begin{aligned} \frac{d}{dt} N_{n,i} = & -N_{n,i} A_{n,i} + \sum_{j \geq i} B_{p \rightarrow n,ji} N_{p,j} + \\ & + \sum_{j \geq i} B_{n \rightarrow n,ji} N_{n,j} + Q_{n,i}, \quad (7) \end{aligned}$$

where

$$Q_{p(n),i} = \int_{E_{i-1/2}}^{E_{i+1/2}} Q_{p(n)}(E) dE, \quad (8)$$

the coefficients  $A_{p(n),i}$  have the physical meaning of interaction rates and are given by

$$\begin{aligned} A_{p,i} &= \int d\epsilon n(\epsilon) \int d\mu \frac{1 - \beta_{p,i}\mu}{2} \times \\ &\quad \times [\sigma_{p,\pi}(E_i, \epsilon, \mu) + \sigma_{p,e}(E_i, \epsilon, \mu)], \\ A_{n,i} &= \int d\epsilon n(\epsilon) \int d\mu \frac{1 - \beta_{n,i}\mu}{2} \sigma_{n,\pi}(E_i, \epsilon, \mu) + \\ &\quad + \frac{m_n}{E_{n,i}} \tau_n^{-1}, \end{aligned} \quad (9)$$

and the coefficients  $B_{x \rightarrow y,ji}$  are given by

$$\begin{aligned} B_{p \rightarrow p,ji} &= \int d\epsilon n(\epsilon) \int d\mu \frac{1 - \beta_{p,j}\mu}{2} \int_{E_{i-1/2}}^{E_{i+1/2}} dE_p \times \\ &\quad \times \left[ \frac{d\sigma_{p,\pi}}{dE_p}(E_j, \epsilon, \mu; E_p) + \frac{d\sigma_{p,e}}{dE_p}(E_j, \epsilon, \mu; E_p) \right], \end{aligned} \quad (10)$$

$$\begin{aligned} B_{p \rightarrow n,ji} &= \int d\epsilon n(\epsilon) \int d\mu \frac{1 - \beta_{p,j}\mu}{2} \int_{E_{i-1/2}}^{E_{i+1/2}} dE_n \times \\ &\quad \times \frac{d\sigma_{p,\pi}}{dE_n}(E_j, \epsilon, \mu; E_n), \end{aligned}$$

$$\begin{aligned} B_{n \rightarrow p,ji} &= \int d\epsilon n(\epsilon) \int d\mu \frac{1 - \beta_{n,j}\mu}{2} \int_{E_{i-1/2}}^{E_{i+1/2}} dE_p \times \\ &\quad \times \frac{d\sigma_{n,\pi}}{dE_p}(E_j, \epsilon, \mu; E_p) + \delta_j^i \frac{m_n}{E_i} \tau_n^{-1}, \end{aligned}$$

$$\begin{aligned} B_{n \rightarrow n,ji} &= \int d\epsilon n(\epsilon) \int d\mu \frac{1 - \beta_{n,j}\mu}{2} \int_{E_{i-1/2}}^{E_{i+1/2}} dE_n \times \\ &\quad \times \frac{d\sigma_{n,\pi}}{dE_n}(E_j, \epsilon, \mu; E_n). \end{aligned}$$

The system of ordinary differential equations (ODE) (6) and (7) can be solved using standard methods. The TransportCR code utilizes the GNU Scientific Library (GSL), which provides a choice of 11 adaptive step ODE integration schemes. In addition to standard GSL schemes, a first-order implicit scheme is implemented in the code, which benefits the observation

that the matrixes  $B_{x \rightarrow y,ji}$  in Eqs. (6) and (7) are triangular. This makes it possible to speed up the ODE solving by reducing the number of independent variables. The implicit method has the advantage that the solution converges even for a relatively large time step. However, to ensure the desired accuracy, we need to optimize the step size for a given problem by trial and error. We note that the coefficients  $A_{x,i}$  and  $B_{x \rightarrow y,ji}$  depend on time because of the redshift dependence of the background concentration. In general, the step size should be proportional to the interaction length  $A_{p(n),i}^{-1}$  and the length itself is inversely proportional to the concentration of background photons, and we therefore make the time step dependent on  $z$ :

$$h(z) = h(0)(1+z)^{-3}, \quad (11)$$

which corresponds to the evolution of the CMB photon concentration. There is no need to recalculate the coefficients  $A_{x,i}$  and  $B_{x \rightarrow y,ji}$  before each step unless the background is highly variable. In practice, we recalculate the coefficients after time intervals corresponding to the redshift change of one log bin:

$$\frac{z_i + 1}{z_{i+1} + 1} = 10^{1/n_d}. \quad (12)$$

The same calculation technique is used to obtain the fluxes of secondary particles produced by nucleons: electrons, positrons, photons, and neutrinos. The electron-photon cascade is driven by a chain of inverse Compton scattering and  $e^+e^-$  pair production by photons, while secondary neutrinos propagate practically without attenuation. The direct application of the above scheme may be difficult in the special case of the fast processes with small inelasticity since it would require the high density of energy binning and small time steps. The  $e^+e^-$  pair production by protons is a good example of such a process having the inelasticity less than  $10^{-3}$ . A similar problem occurs in the Monte Carlo simulation method. In both techniques, the continuous energy loss approximation is used to bypass the problem with the mean energy loss rate given by the equation

$$\begin{aligned} -\frac{dE}{dt} &= \int d\epsilon n(\epsilon) \int d\mu \frac{1 - \beta\mu}{2} \times \\ &\quad \times \int dE'(E - E') \frac{d\sigma}{dE'}(E, \epsilon, \mu; E'). \end{aligned} \quad (13)$$

In Monte Carlo simulations, the CEL implementation is straightforward, but in the transport equation approach, a simple first-order scheme is used to express

continuous energy loss in terms of the coefficients  $A_{x,i}$  and  $B_{x \rightarrow x,ji}$  in Eqs. (6) and (7):

$$A_{x,i} = \frac{1}{E_i - E_{i-1}} \left. \frac{dE}{dt} \right|_{E=E_{i-1/2}}, \quad (14)$$

$$B_{x \rightarrow x,ji} = \delta_j^{i+1} A_{x,j}.$$

Equations (6) and (7) do not take expansion of the universe into account. One way to treat it would be to introduce the CEL term with

$$-\frac{dE}{dt} = -\frac{dE}{dz} \frac{dz}{dt} = \frac{E}{1+z} H_0 (1+z) \sqrt{\Omega_m (1+z)^3 + \Omega_\Lambda} \quad (15)$$

along with replacing  $Q_x(E)$  with comoving source densities  $\tilde{Q}_x(E, z) = (1+z)^{-3} Q_x(E)$  in (8) to take the volume increase into account. As an alternative to the introduction of an extra CEL term, one could shift the energy binning each step (12), as is done in Ref. [18]. Both methods agree in the limit of large  $n_d$ , the former is more accurate in the presence of other more rapid attenuation channels, while the latter is precise in the absence of any interactions.

### 2.2.1. Photopion production

Photopion production is the main attenuation mechanism for protons and neutrons with energies  $E \gtrsim 10$  EeV. The energy threshold for this process is

$$E_{th} = \frac{2m_N m_\pi + m_\pi^2}{4\epsilon} \approx 6.8 \left( \frac{\epsilon}{10^{-3} \text{ eV}} \right)^{-1} \text{ EeV}, \quad (16)$$

where  $m_N$  is the nucleon mass. This process was extensively studied in Ref. [42], where the SOPHIA event generator was developed for simulation of photopion production including the calculation of various channel cross sections and sampling of secondaries. Both CRPropa and the transport-equation-based code use the SOPHIA event generator as black box. The former code calls the event generator directly, while the latter provides an auxiliary routine to calculate the propagation coefficients  $A_{x,i}$  and  $B_{x \rightarrow y,ji}$  using calls of SOPHIA procedures, as is described below. We first rewrite the contribution from photopion production in Eqs. (9) and (10) in terms of the photon energy  $\tilde{\epsilon}$  in the nucleon rest frame (NRF),

$$\tilde{\epsilon} = \frac{\epsilon E_N}{m_N} (1 - \beta\mu) \equiv \epsilon\gamma(1 - \beta\mu), \quad (17)$$

where  $E_N$  is the nucleon energy, and  $\gamma = E_N/m_N$ . The threshold energy for photopion production is

$$\tilde{\epsilon}_{th} = \frac{m_\pi^2 + 2m_\pi m_N}{2m_N} \approx 0.15 \text{ GeV}. \quad (18)$$

After omitting the terms related to pair production and neutron decay in (9) and (10), in the ultrarelativistic limit ( $\beta \rightarrow 1$ ), we have

$$A_{p(n),i} = \frac{1}{2\gamma_i^2} \int_{\tilde{\epsilon}_{th}}^{2\gamma_i \epsilon_{max}} d\tilde{\epsilon} I_b \left( \frac{\tilde{\epsilon}}{2\gamma} \right) \tilde{\epsilon} \sigma_{p(n)}(\tilde{\epsilon}), \quad (19)$$

$$B_{x \rightarrow y,ji} = \frac{1}{2\gamma_i^2} \int_{\tilde{\epsilon}_{th}}^{2\gamma_i \epsilon_{max}} d\tilde{\epsilon} I_b \left( \frac{\tilde{\epsilon}}{2\gamma} \right) \tilde{\epsilon} \int_{E_{i-1/2}}^{E_{i+1/2}} dE_y \times \frac{d\sigma_x}{dE_y}(\tilde{\epsilon}, E_j; E_y), \quad (20)$$

where  $\epsilon_{max}$  is the maximal photon background energy in the laboratory frame and

$$I_b(\epsilon_{th}) = \int_{\epsilon_{th}}^{\epsilon_{max}} \frac{n(\epsilon) d\epsilon}{\epsilon^2} \quad (21)$$

is an integral depending solely on the photon background density and can be tabulated. The total photopion production cross sections as functions of the NRF photon energy  $\sigma_{p(n)}(\tilde{\epsilon})$  are explicitly implemented in SOPHIA, which suffices for the  $A_{p(n),i}$  coefficients calculation.

To calculate  $B_{x \rightarrow y,ji}$ , we create a logarithmic binning in  $\tilde{\epsilon}$  with  $n_d$  steps per decade from  $\tilde{\epsilon}_{th}$  given by (18) and  $\tilde{\epsilon}_{max} = 2\epsilon_{max}\gamma_{max}$  and for each  $\tilde{\epsilon}_i$  in the NRF, we perform sampling of secondary particles for  $10^5$ – $10^6$  times. We assume that the nucleon momentum  $p_N$  in the laboratory frame is directed along the  $z$  axis. Then because  $p_N \gg \epsilon$ , the NRF background photon momentum  $\tilde{\epsilon}$  should point to the opposite direction. Let  $\tilde{E}'$  and  $\tilde{p}'_z$  be the energy and the  $z$ -component of the sampled secondary particle momentum in the NRF. Then its energy in the laboratory frame is

$$E' = \gamma(\tilde{E}' + \beta\tilde{p}'_z). \quad (22)$$

Therefore, in the ultrarelativistic limit ( $\beta \rightarrow 1$ ) we have

$$r \equiv \frac{E'}{E_N} = \frac{\tilde{E}' + \tilde{p}'_z}{m_N}. \quad (23)$$

It follows from Eq. (23) that the distribution  $p(r)$  of the random variable  $r$  does not depend on the primary nucleon energy  $E_N$  and may solely depend on  $\tilde{\epsilon}$ . Therefore, for the construction of  $B_{x \rightarrow y,ji}$ , it is enough to build the 2D tables of  $p_{x \rightarrow y}(r; \tilde{\epsilon})$  for each pair of primary and secondary particles. If the distribution functions  $p_{x \rightarrow y}(r; \tilde{\epsilon})$  are normalized to the average total number of secondary particles of type  $y$  produced

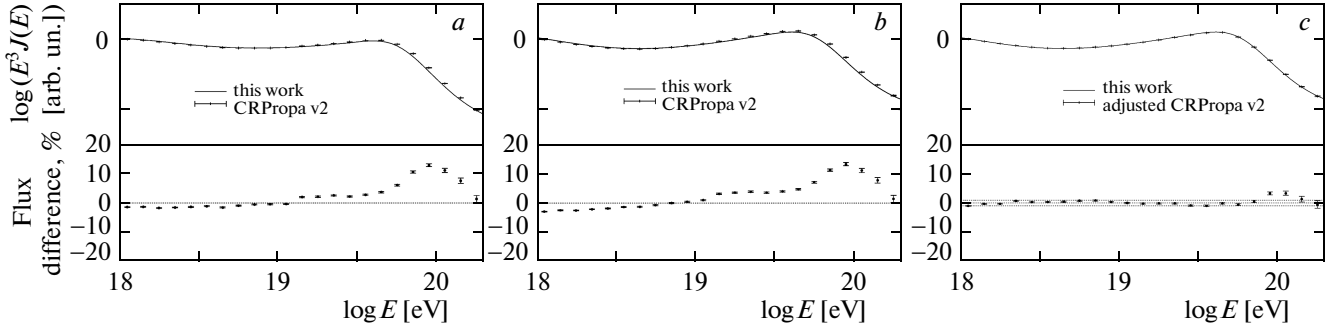


**Fig. 1.** Propagated spectra calculated by CRPropa ver.2 (black dots) and kinetic equation based code with binning density  $n_d = 100$  (solid red line) for the source model parameters  $m = 0, p = 2.69$  (a);  $m = 4, p = 2.4$  (b); improved,  $m = 4, p = 2.4$  (c) and assuming extragalactic background light (EBL) model of Ref. [35]. Lower panels show relative difference in the spectra predictions. Figures *a, b* were obtained using original CRPropa ver.2 while for Fig. *c* the corrected version of CRPropa was used. Also 1% error band is shown in Fig. *c* in pink. (Color on-line see arXiv:1406.0735)

by primary particles of type  $x$  in collision with a photon  $\tilde{\epsilon}$ , then

$$B_{x \rightarrow y, ji} = \frac{1}{2\gamma_i^2} \int_{\tilde{\epsilon}_{th}}^{2\gamma_i \epsilon_{max}} d\tilde{\epsilon} I_b \left( \frac{\tilde{\epsilon}}{2\gamma} \right) \tilde{\epsilon} \sigma_x(\tilde{\epsilon}) \times \int_{E_{i-1/2}/E_j}^{E_{i+1/2}/E_j} dr p_{x \rightarrow y}(r; \tilde{\epsilon}). \quad (24)$$

In practice, the routine tabulates fractions of events with  $r$  falling to a given range:

$$P_{l,k} = \frac{\int_{10^{-(l-1/2)/n_d}}^{10^{-(l+1/2)/n_d}} dr p_{x \rightarrow y}(r; \tilde{\epsilon}_k) \equiv \frac{N_{l,k}}{N_{tot,k}}. \quad (25)$$

### 2.2.2. $e^+e^-$ pair production by protons

The  $e^+e^-$  pair production is the main energy attenuation mechanism for protons with energies below the GZK cutoff. The energy threshold for this process is

$$E_{th} = \frac{m_e(m_p + m_e)}{\epsilon} \approx 0.5 \left( \frac{\epsilon}{10^{-3} \text{ eV}} \right)^{-1} \text{ EeV}. \quad (26)$$

As was mentioned above, the process is characterized by low inelasticity, and therefore the CEL approximation is used. The energy loss rate for the process on an arbitrary isotropic background was calculated in Ref. [43] (see formulas (3.11)–(3.19)).

### 3. COMPARISON OF THE SIMULATION RESULTS

In this section, we use a simple phenomenological model for source evolution and the injection spectrum to compare the simulations described above:

$$\frac{d\Phi}{dt dE} \propto E^{-p} (1+z)^{3+m}, \quad (27)$$

$$E < 10^{21} \text{ eV}, \quad z < 4.$$

In Fig. 1, we show calculation results for the propagated spectra in two numerical codes. We consider both sources with constant density (Fig. 1a) and the sources with strong evolution (Fig. 1b). The highest discrepancy is observed in the latter case. It reaches 14% at the super-GZK energy. Nevertheless, the effect of this discrepancy on the spectrum fitting is weaker than that of the uncertainty in the sub-GZK energy region, where more statistics is available. In this region, the difference in the flux predictions is at most 4%. In the case of a nonevolving source, the discrepancy is less pronounced. The above observations naturally lead to the assumption that the differences may be related to pion production and in particular to the implementation of this process for  $z > 0$ .

In Fig. 2, we compare the energy loss rates for  $e^+e^-$  pair production and the interaction lengths for pion production (see Fig. 2) at the redshift  $z = 1$ .

The discrepancy is clearly seen for both processes in Fig. 2, although in the case of pair production, it should not have effect on the spectrum since the energy loss lengths become different in the region where redshift is the main attenuation mechanism. In fact, the discrepancy is caused by the simplifying assump-

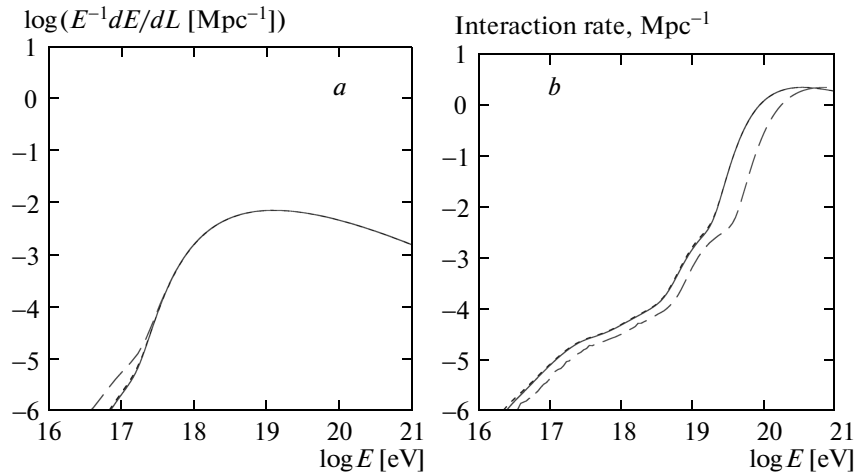


**Fig. 2.** Comparison of rate calculations between two programs. The energy loss rate for  $e^+e^-$  pair production process (a) and interaction rate for pion production process (b) calculated for  $z = 1$ . Rates obtained in CRPropa ver.2 are shown by dashed green lines, the rates calculated in transport equation code shown by solid red lines and the rates recalculated in CRPropa after corrections described in the text are shown by dotted blue lines (EBL model of Ref. [35] is assumed). (Color on-line see arXiv:1406.0735)

tion on the dependence of the energy loss rate on  $z$  used in CRPropa,

$$\frac{1}{E} \frac{dE}{dt}(E, z) = (1+z)^3 \frac{1}{E} \frac{dE}{dt}(E(1+z), z=0), \quad (28)$$

which is only valid for the CMB background.

The difference in the pion production interaction length is more important. In the CRPropa code, pion production on the CMB is implemented using prebuilt interaction rate tables for  $z = 0$  and scaling with redshift according to a formula similar to (28), while interaction rates on the infrared background are calculated for each  $z$  in the same way as the pion production term in formula (9), namely, by integrating the collision-angle-averaged cross section (which is tabulated) with the photon background spectrum. After inspecting the CRPropa code and the tables, we came to the conclusion that the cross section function should be tabulated for a broader range of arguments, and the integration procedure accuracy as well as the interpolation of cross section tables can be enhanced. With the above corrections implemented, we have also rebuilt the interaction rate table for the CMB background. In Fig. 2, the corrected rates are shown as well. We have also implemented a more precise calculation of the pair production energy loss rates in CRPropa taking the evolution of the infrared background into account in a proper way.

Figure 1c illustrates the level of agreement achieved after applying corrections to the CRPropa code in the

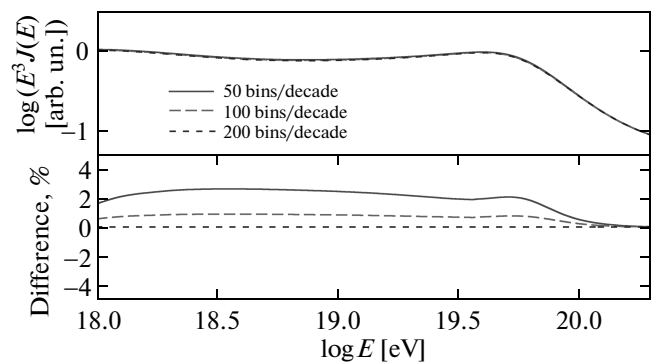


**Fig. 3.** Comparison of TransportCR simulations with various binning densities in the model (27) with  $m = 0$  and  $p = 2.69$ . (Color on-line see arXiv:1406.0735)

case of strong source evolution. We note that in the case of a nonevolving source, the same level of accuracy is achieved. The calculation of the spectra presented in Fig. 1 took 60 hours of a 2.2 GHz CPU time using CRPropa and 0.6 hours of the CPU time using the Transport code with 100 points per decade binning. Figure 3 illustrates the dependence of the TransportCR code calculation accuracy on the binning density. The difference between 100 and 200 points per decade runs is at level below 1 %, which is less than or comparable to the discrepancy between the predictions of the two codes discussed above. We therefore conclude that for the current level of consistency, it is enough to use 100

points per decade binning in the TransportCR code.

We have compared the results of simulating ultra-high-energy nucleon propagation using the CRPropa and TransportCR codes and suggested improvements to the procedure of the interaction rate calculation in CRPropa. After applying the suggested improvements, we have achieved a 1 % level of agreement in flux predictions by the two codes for the whole relevant energy range except a small interval in the super-GZK region  $10^{19.9} \leq E \leq 10^{20.1}$ , where the relative error grows to 3 %. The level of accuracy achieved is enough for a consistent analysis of the latest UHECR data. We have applied the propagation codes described above to fit the Telescope Array experimental spectrum [44] assuming phenomenological source model (27). The enhancements in CRPropa introduced in this work allow achieving the systematic uncertainty in the best fit parameters related to the choice of the propagation code at the level of  $\Delta p \approx 0.01$  and  $\Delta m \approx 0.1$ . The modified CRPropa and Transport code described in this work can be downloaded from [45]. The modifications suggested in the former code have been discussed with the CRPropa development team and will be incorporated into the CRPropa 3 release version [46].

We thank M. Fukushima, K. Kawata, H. Sagawa, G. Sigl, and I. Tkachev for the fruitful discussions. The work of O. K. was supported by the Russian Federal Science Fund grant RSCF 14-12-01340.

## REFERENCES

1. T. Abu-Zayyad, R. Aida, M. Allen et al., *Astrophys. J. Lett.* **768**, L1 (2013) [arXiv:1205.5067 [astro-ph.HE]].
2. The Pierre Auger Collaboration, *Phys. Rev. Lett.* **101**, 061101 (2008).
3. R. U. Abbasi et al., *Phys. Rev. Lett.* **100**, 101101 (2008).
4. K. Greisen, *Phys. Rev. Lett.* **16** (1966).
5. G. T. Zatsepin and V. A. Kuz'min, *Sov. Phys. JETP Lett.* **4**, 78 (1966).
6. J. Abraham et al., *Phys. Rev. Lett.* **104**, 091101 (2010).
7. R. U. Abbasi et al., *Phys. Rev. Lett.* **104**, 161101 (2010).
8. T. Abu-Zayyad et al. [Telescope Array and Pierre Auger Collaborations], arXiv:1310.0647 [astro-ph.HE].
9. V. S. Berezhinsky and S. I. Grigor'eva, *Astron. Astrophys.* **199**, 1 (1988).
10. F. A. Aharonian, B. L. Kanevsky, and V. V. Vardanian, *Astrophys. Space Sci.* **167**, 93 (1990).
11. J. P. Rachen and P. L. Biermann, *Astron. Astrophys.* **272**, 161 (1993).
12. J. Geddes, T. C. Quinn, and R. M. Wald, *Astrophys. J.* **459**, 384 (1996).
13. E. Waxman, *Astrophys. J. Lett.* **452**, L1 (1995).
14. L. A. Anchordoqui, M. T. Dova, L. N. Epele, and J. D. Swain, *Phys. Rev. D* **55**, 7356 (1997).
15. V. Berezhinsky, A. Z. Gazizov, and S. I. Grigorieva, *Phys. Rev. D* **74**, 043005 (2006) [arXiv:hep-ph/0204357].
16. S. Yoshida and M. Teshima, *Progr. Theor. Phys.* **89**, 883 (1993).
17. C. T. Hill and D. N. Schramm, *Phys. Rev. D* **31**, 564 (1985).
18. S. Lee, *Phys. Rev. D* **58**, 043004 (1998) [arXiv:astro-ph/9604098].
19. O. K. Kalashev, PhD thesis, Institute for Nuclear Research RAS, Moscow (2003); G. B. Gelmini, O. Kalashev, and D. V. Semikoz, *JCAP* **1201**, 044 (2012) [arXiv:1107.1672 [astro-ph.CO]]; K. Arisaka, G. B. Gelmini, M. D. Healy, O. E. Kalashev, and J. Lee, *JCAP* **0712**, 002 (2007) [arXiv:0709.3390 [astro-ph]].
20. R. Aloisio, D. Boncioli, A. F. Grillo, S. Petrera, and F. Salamida, *JCAP* **1210**, 007 (2012) [arXiv:1204.2970 [astro-ph.HE]].
21. F. A. Aharonian and J. W. Cronin, *Phys. Rev. D* **50**, 1892 (1994).
22. J. W. Elbert and P. Sommers, *Astrophys. J.* **441**, 151 (1995).
23. G. Sigl, M. Lemoine, and A. Olinto, *Phys. Rev. D* **56**, 4470 (1997).
24. D. Allard, E. Parizot, E. Khan, S. Goriely, and A. V. Olinto, *Astron. Astrophys.* **443**, L29 (2005) [arXiv:astro-ph/0505566].
25. K.-H. Kampert, Jr. Kulbartz, L. Maccione, N. Nierstenhoefer, P. Schiffer, G. Sigl, and A. R. van Vliet, *Astropart. Phys.* **42**, 41 (2013) [arXiv:1206.3132 [astro-ph.IM]]; R. A. Batista, M. Erdmann, C. Evoli et al., arXiv:1307.2643 [astro-ph.IM].

26. A. A. Lagutin and V. V. Uchaikin, *Izv. Altai. Gos. Univ.* **9**, 4 (1998).
27. J. L. Puget, F. W. Stecker, and J. H. Bredekamp, *Astrophys. J.* **205**, 638 (1976).
28. L. N. Epele and E. Roulet, *Phys. Rev. Lett.* **81**, 3295 (1998); *J. High Energy Phys.* **9810**, 009 (1998).
29. F. W. Stecker and M. H. Salamon, *Astrophys. J.* **512**, 521 (1999).
30. A. Aab et al. [Pierre Auger Collaboration], arXiv:1307.5059 [astro-ph.HE].
31. R. Durrer and A. Neronov, *Astron. Astrophys. Rev.* **21**, 62 (2013) [arXiv:1303.7121 [astro-ph.CO]].
32. K. Dolag, D. Grasso, V. Springel, and I. Tkachev, *JCAP* **0501**, 009 (2005) [arXiv:astro-ph/0410419].
33. G. Sigl, F. Miniati, and T. A. Ensslin, arXiv:astro-ph/0309695.
34. V. Berezhinsky and A. Z. Gazizov, *Astrophys. J.* **669**, 684 (2007) [arXiv:astro-ph/0702102 [ASTRO-PH]].
35. T. M. Kneiske et al., *Astron. Astrophys.* **386**, 1 (2002); *ibid.*, **413**, 807 (2004).
36. A. Franceschini, G. Rodighiero, and M. Vaccari, *Astron. Astrophys.* **487**, 837 (2008) [arXiv:0805.1841 [astro-ph]].
37. F. W. Stecker, M. A. Malkan, and S. T. Scully, *Astrophys. J.* **648**, 774 (2006).
38. T. M. Kneiske and H. Dole, arXiv:1001.2132 [astro-ph.CO].
39. F. W. Stecker, M. A. Malkan, and S. T. Scully, *Astrophys. J.* **761**, 128 (2012); S. T. Scully, M. A. Malkan, and F. W. Stecker, arXiv:1401.4435 [astro-ph.HE].
40. Y. Inoue et al., arXiv:1212.1683.
41. F. W. Stecker and M. H. Salamon, *Astrophys. J.* **512**, 521 (1999) [arXiv:astro-ph/9808110].
42. A. Mucke, R. Engel, J. P. Rachen, R. J. Protheroe, and T. Stanev, *Comput. Phys. Comm.* **124**, 290 (2000) [arXiv:astro-ph/9903478].
43. M. J. Chodorowski, A. A. Zdziarski, and M. Sikora, *Astrophys. J.* **400**, 181 (1992).
44. Telescope Array collaboration, in preparation.
45. Transport code and modified CRPropa code, <http://sourceforge.net/projects/transportcr/files/>.
46. G. Sigl, private communication.